

Human Pose Regression by Combining Indirect Part Detection and Contextual Information

Diogo C. Luvizon

Hedi Tabia

David Picard

ETIS Lab., UMR 8051, Université Paris Seine,
Université Cergy-Pontoise, ENSEA, CNRS.

{diogo.luvizon, hedi.tabia, picard}@ensea.fr

Abstract

In this paper, we propose an end-to-end trainable regression approach for human pose estimation from still images. We use the proposed Soft-argmax function to convert feature maps directly to joint coordinates, resulting in a fully differentiable framework. Our method is able to learn heat maps representations indirectly, without additional steps of artificial ground truth generation. Consequently, contextual information can be included to the pose predictions in a seamless way. We evaluated our method on two very challenging datasets, the Leeds Sports Poses (LSP) and the MPII Human Pose datasets, reaching the best performance among all the existing regression methods and comparable results to the state-of-the-art detection based approaches.

1. Introduction

Human pose estimation from still images is a hard task since the human body is strongly articulated, some parts may not be visible due to occlusions or low quality images, and the visual appearance of body parts can change significantly from one pose to another. Classical methods use keypoint detectors to extract local information, which are combined to build pictorial structures [16]. To handle difficult cases of occlusion or partial visualization, contextual information is usually needed to provide visual cues that can be extracted from a broad region around the part location [15] or by interaction among detected parts [45]. In general, pose estimation can be seen from two different perspectives, namely as a correlated part detection problem or as a regression problem. Detection based approaches commonly try to detect keypoints individually, which are aggregated in post-processing stages to form one pose prediction. In contrast, methods based on regression use a function to map directly input images to body joint positions.

In the last few years, pose estimation have gained attention with the breakthrough of deep Convolutional Neural

Networks (CNN) [42] alongside consistent computational power increase. This can be seen as the shift from classical approaches [32, 25] to deep architectures. In many recent works from different domains, CNN based methods have overcome classical approaches by a large margin [18, 37]. A key benefit from CNN is that the full pipeline is differentiable, allowing end-to-end learning. In the context of human pose estimation, the first methods using deep neural networks tried to do regression directly by learning a non-linear mapping function from RGB images to joint coordinates [42]. By contrast, the majority of the methods in the state of the art tackle pose estimation as a detection problem by predicting heat maps that corresponds to joint locations [27, 5]. In such methods, the ground truth is artificially generated from joint positions, generally as a 2D Gaussian distribution centered on the joint location, while the context information is implicitly learned by the hidden convolutional layers.

Despite achieving state-of-the-art accuracy on 2D pose estimation, detection based approaches have some limitations. For example, such methods relies on additional steps to convert heat maps to joint positions, usually by applying the *argmax* function, which is not differentiable, breaking the learning chain on neural networks. Additionally, the precision of predicted keypoints is proportional to that of the heat map resolution, which leads the top ranked methods [13, 27] to high memory consumption and high computational requirements.

Moreover, regression based methods are conceptually more adapted to 2D and 3D scenarios and can be used indistinctly on both cases [36, 38]. However, the regression function map is sub-optimally learned, resulting in lower results if compared to detection based approaches. In this paper, we aim at solving this problem by bridging the gap between detection and regression based methods. We propose to replace the *argmax* function, used to convert heat maps into joint locations, by what we call the *Soft-argmax* function, which keeps the properties of specialized part detectors while being fully differentiable. With this solution,

we are able to optimize our model from end-to-end using regression losses, *i.e.*, from input RGB images to final (x, y) body joint coordinates.

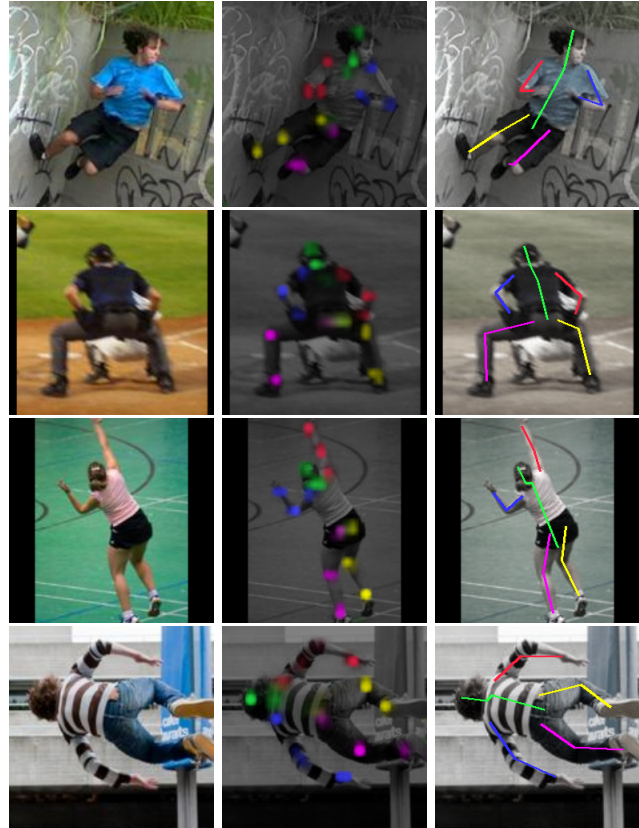
The contributions of our work are the following: first, we present a human pose regression approach from still images based on the *Soft-argmax* function, resulting in an end-to-end trainable method which does not require artificial heat maps generation for training. Second, the proposed method can be trained using an insightful regression loss function, which is directly linked to the error distance between predicted and ground truth joint positions. Third, in the proposed architecture, contextual information is directly accessible and is easily aggregated to the final predictions. Finally, the accuracy reached by our method surpasses that of regression methods and is close to that of state-of-the-art detection methods, despite using a much smaller network. Some examples of our regressed poses are shown in Fig. 1. Additionally, we provide our implementation of the proposed method in Python using the open source Keras library [10].¹

The rest of this paper is divided as follows. In the next section, we present a review of the most relevant related work. The proposed method is presented in Section 3. In Section 4, we show the experimental evaluations, followed by our conclusions in Section 5.

2. Related work

Several approaches for human pose estimation have been presented for both 2D [14, 26] and 3D [22] scenarios, as well as for video sequences [29]. Among classical methods, Pictorial Structures [2] and poselet-based features [31] have been widely used in the past. In this section, due to limited space, we focus on CNN based methods that are more related to our work. We briefly refer to the most recent works, splitting them as regression based and detection based approaches.

Regression based approaches. Some methods tackled pose estimation as a keypoint regression problem. One of the first regression approaches was proposed by Toshev and Szegedy [42] as a holistic solution based on cascade regression for body part detection, where individual joint positions are recursively improved, taking the full frame as input. Pfister *et al.* [30] proposed the Temporal Pose ConvNet to track upper body parts, and Carreira *et al.* [6] proposed the Iterative Error Feedback by injecting the prediction error back to the input space, improving estimations recursively. Recently, Sun *et al.* [38] proposed a structured bone based representation for human pose, which is statistically less variant than absolute joint positions and can be indistinctly used for both 2D and 3D representations. However, the



(a) Input image (b) Part-based maps (c) Pose

Figure 1: Test samples from the Leeds Sports Poses (LSP) dataset. Input image (a), the predicted part-based maps encoded as RGB image for visualization (b), and the regressed pose (c). Corresponding human limbs have the same colors in all images. This figure is better seen in color.

method requires converting pose data to the relative bone based format. Moreover, those results are all outperformed by detection based methods.

Detection based approaches. Pischulin *et al.* [33] proposed DeepCut, a graph cutting algorithm that relies on body parts detected by DeepPose [42]. This method has been improved in [21] by replacing the previous CNN by a deep Residual Network (ResNet) [19], resulting in very competitive accuracy results, specially on multi-person detection. More recent methods have shown significant improvements on accuracy by using fully convolutional models to generate belief maps (or heat maps) for joint probabilities [34, 3, 5, 27, 13]. For example, Bulat *et al.* [5] proposed a two-stages CNN for coarse and fine heat map regression using pre-trained models, and Gkioxari *et al.* [17] presented a structured prediction method, where the prediction of each joint depends on the intermediate feature maps and the distribution probability of the previously pre-

¹ The Python source code will be publicly available after acceptance at <https://github.com/dluvizon/pose-regression>.

dicted joints. Following the tendency of deeper models with residual connections, Newell *et al.* [27] proposed a stacked hourglass network with convolutions in multi-level features, allowing reevaluation of previous estimations due to a stacked block architecture with many intermediate supervisions. The part-based learning process can benefit from intermediate supervision because it acts as constraints on the lower level layers. As a result, the feature maps on higher levels tend to be cleaner. Recently, Chu *et al.* [13] extended the stacked hourglass network by increasing the network complexity and using a CRF based attention map alongside intermediate supervisions to reinforce the task of learning structural information. These results provide to our knowledge state-of-the-art performance.

All the previous methods that are based on detection need additional steps on training to produce artificial ground truth from joint positions, which represent an additional processing stage and additional hyper-parameters, since the ground truth heat maps have to be defined by hand. On evaluation, the inverse operation is required, *i.e.*, heat maps have to be converted to joint positions, generally using the *argmax* function. Consequently, in order to achieve good precision, predicted heat maps need reasonable spacial resolution, which increases quadratically the computational cost and memory usage. In order to provide an alternative to heat maps based approaches, we present our framework in the following section.

3. Proposed method

The proposed approach is an end-to-end trainable network which takes as input RGB images and outputs two vectors: the probability \mathbf{p}_n of joint n being in the image and the regressed joint coordinates $\mathbf{y}_n = (x_n, y_n)$, where $n = \{1, 2, \dots, N_J\}$ is the index of each joint and N_J is the number of joints. In what follows, we first present the global architecture of our method, and then detail its most important parts.

3.1. Network architecture

An overview of the proposed method is presented in Fig. 2. Our approach is based on a convolutional neural network essentially composed of three parts: one entry flow (Stem), Block-A and Block-B. The role of the stem is to provide basic feature extraction, while Block-A provides refined features and Block-B provides body-part and contextual activation maps. One sequence of Block-A and Block-B is used to build one *prediction block*, which output is used as intermediate supervision during training. The full network is composed by the stem and a sequence of K prediction blocks. The final prediction is the output of the K^{th} prediction block. To predict the pose at each prediction block, we aggregate the 2D coordinates generated by applying *Soft-argmax* to the part-based and contextual

maps that are output by Block-B. Similarly to recent approaches [27, 13], on each prediction block we produce one estimation that is used as intermediate supervision, providing better accuracy and more stability to the learning process. As a convention, we use the generic term “heat map” to refer both to part-based and contextual feature maps, since these feature maps converge to heat maps like representations.

The proposed CNN model is partially based on Inception-v4 [39] and on the Stacked Hourglass [27] networks. We also inspired our model on the “extreme” inception (Xception) [9] network, which relies on the premise that convolutions can be separated into spatial convolutions (individual for each channel) followed by a 1×1 convolution for cross-channel projection, resulting in significant reduction on the number of parameters and on computations. This idea is called *depthwise separable convolution* (SepConv) and an optimized implementation is available on the TensorFlow framework.

In our network, the “Stem” is based on Inception-v4’s stem followed by a SepConv layer in parallel with a shortcut layer, as presented in Fig. 3a. For Block-A, we use a similar architecture as the Stacked Hourglass replacing all the residual blocks by a residual separable convolution (Res-SepConv), as depicted in Fig. 3b. Additionally, our approach increased the results from [27] with only three feature map resolutions, from 32×32 to 8×8 , instead of the original five resolutions, from 64×64 to 4×4 .

At each prediction stage, Block-B is used to transform input feature maps into M_d *part-based detection maps* (\mathbf{H}_d) and M_c *context maps* (\mathbf{H}_c), resulting in $M = M_d + M_c$ heat maps. For the specific problem of pose estimation, M_d corresponds to the number of joints N_J , and $M_c = N_c N_J$, where N_c is the number of context maps for each joint. The produced heat maps are projected back to the feature space and reintroduced to the network flow by a 1×1 convolution. Similar techniques have been used by many previous works [5, 27, 13], resulting in significant gain of performance. From the generated heat maps, our method computes the predicted joint locations and joint probabilities in the regression block, which has no trainable parameters. The architecture of Block-B and the regression stage is shown in Fig. 4.

3.2. Proposed regression method

As presented in Section 2, traditional regression based methods use fully connected layers on feature maps and learn the regression mapping. However, this approach usually gives sub-optimal solutions. While state-of-the-art methods are overwhelmingly based on part detection, approaches based on regression have the advantages of providing directly the pose prediction as joint coordinates without additional steps or post-processing. In order to provide an

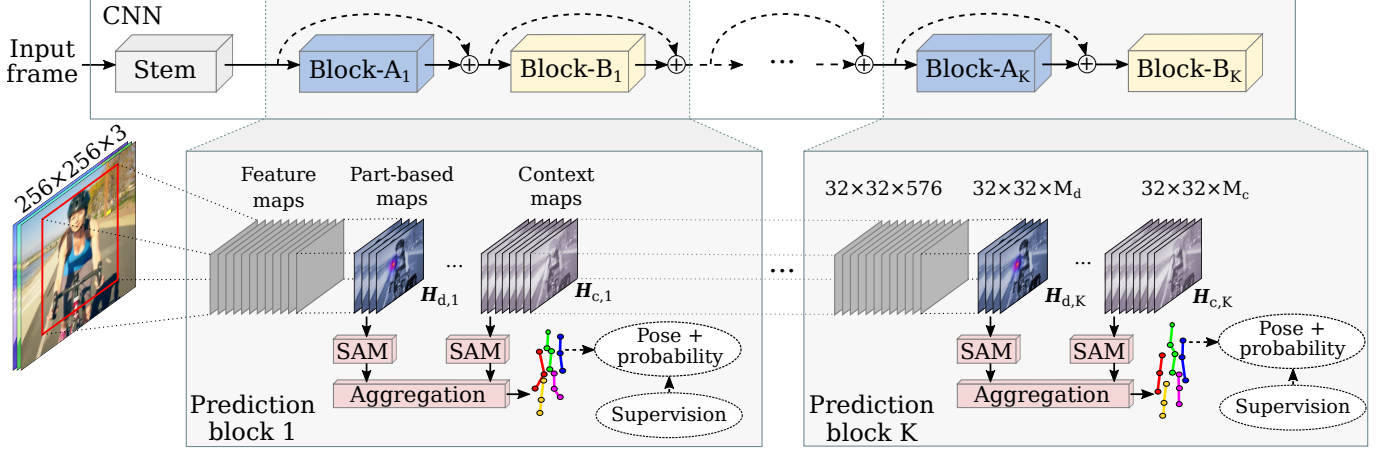


Figure 2: Overview of the proposed approach for pose regression.

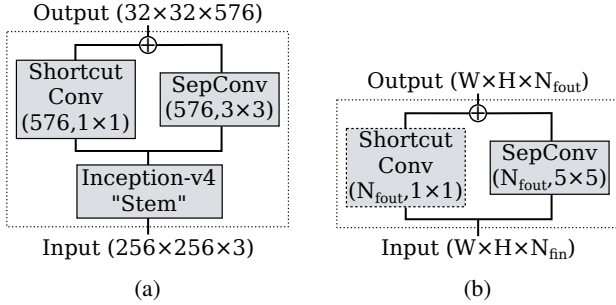


Figure 3: In the proposed network architecture, the Stem (a) is based on Inception-v4’s stem [39] followed by a separable convolution in parallel to a shortcut connection. In (b), we present the residual separable convolution (Res-SepConv), used to replace the residual block in the Stacked Hourglass [27] model. If N_{fin} is equal to N_{fout} , the shortcut convolution is replaced by the identity mapping.

alternative to detection based methods, we propose an efficient and fully differentiable way to convert heat maps directly to (x, y) coordinates, which we call *Soft-argmax*. Additionally, the *Soft-argmax* operation can be implemented as a CNN layer, as detailed in the next section.

3.2.1 Soft-argmax layer

Let us define the *Softmax* operation on a single heat map $\mathbf{h} \in \mathbb{R}^{W \times H}$ as:

$$\Phi(\mathbf{h}_{i,j}) = \frac{e^{\mathbf{h}_{i,j}}}{\sum_{k=1}^W \sum_{l=1}^H e^{\mathbf{h}_{k,l}}}, \quad (1)$$

where $\mathbf{h}_{i,j}$ is the value of heat map \mathbf{h} at location (i, j) , and $W \times H$ is the heat map size. Contrary to the more common cross-channel softmax, we use here a spatial softmax that

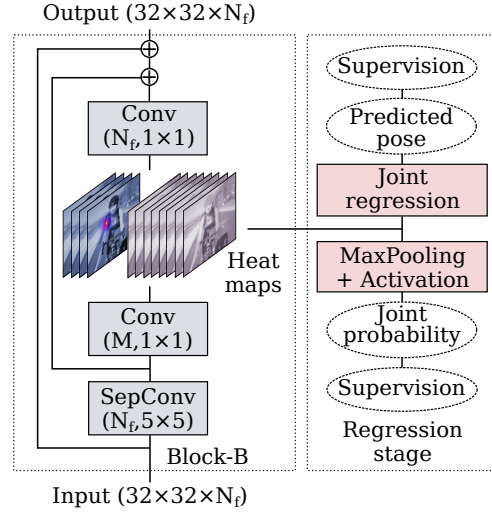


Figure 4: Network architecture of Block-B and an overview of the regression stage. The input is projected into M heat maps ($M_d + M_c$) which are then used for pose regression.

ensures each heat maps is normalized. Then, we define the *Soft-argmax* as follows:

$$\Psi_d(\mathbf{h}) = \sum_{i=1}^W \sum_{j=1}^H \mathbf{W}_{i,j,d} \Phi(\mathbf{h}_{i,j}), \quad (2)$$

where d is a given component x or y , and \mathbf{W} is a $W \times H \times 2$ weight matrix corresponding to the coordinates (x, y) . The matrix \mathbf{W} can be expressed by its components \mathbf{W}_x and \mathbf{W}_y , which are 2D discrete normalized ramps, defined as follows:

$$\mathbf{W}_{i,j,x} = \frac{i}{W}, \mathbf{W}_{i,j,y} = \frac{j}{H}. \quad (3)$$

Finally, given a heat map \mathbf{h} , the regressed location of the predicted joint is given by

$$\mathbf{y} = (\Psi_x(\mathbf{h}), \Psi_y(\mathbf{h}))^T. \quad (4)$$

This *Soft-argmax* operation can be seen as a weighted average of points distributed on an uniform grid, with the weights being equal to the corresponding heat map.

In order to integrate the *Soft-argmax* layer into a deep network, we need its derivative with respect to \mathbf{h} :

$$\frac{\partial \Psi_d(\mathbf{h}_{i,j})}{\partial \mathbf{h}_{i,j}} = \mathbf{W}_{i,j,d} \frac{e^{\mathbf{h}_{i,j}} (\sum_{k=1}^W \sum_{l=1}^H e^{\mathbf{h}_{k,l}} - e^{\mathbf{h}_{i,j}})}{(\sum_{k=1}^W \sum_{l=1}^H e^{\mathbf{h}_{k,l}})^2}. \quad (5)$$

The *Soft-argmax* function can thus be integrated in a trainable framework by using back propagation and the chain rule on equation (5). Moreover, from equation (5), we can see that the gradient is exponentially increasing for higher values, resulting in very discriminative response at the joint position.

The implementation of *Soft-argmax* can be easily done with recent frameworks, such as TensorFlow, just by concatenating a spatial softmax followed by one convolutional layer with 2 filters of size $W \times H$, with fixed parameters according to equation (3).

Unlike traditional *argmax*, *Soft-argmax* provides sub-pixel accuracy, allowing good precision even with very low resolution. Moreover, the *Soft-argmax* operation allows to learn very discriminative heat maps directly from the (x, y) joint coordinates without explicitly computing artificial ground truth. Samples of heat maps learned by our approach are shown in Fig. 5.

3.2.2 Joint probability

Additionally to the joint locations, we estimate the joint probability \mathbf{p}_n , which corresponds to the probability of the n^{th} joint being present in the image. The estimated joint probability is given by the sigmoid activation on the global max-pooling from heat map \mathbf{h}_n . Despite giving an additional piece of information, the joint probability does not depend on additional parameters and is computationally negligible, compared to the cost of convolutional layers.

3.2.3 Detection and context aggregation

Even if the correlation between some joints can be learned in the hidden convolutional layers, the joint regression approach is designed to locate body parts individually, resulting in low flexibility to learn from the context. For example, the same filters that give high response to images of a clean head, also must react positively to a hat or a pair of sunglasses. In order to provide multi-source information to the final prediction, we include in our framework

specialized part-based heat maps and context heat maps, which are defined as $\mathbf{H}_d = [\mathbf{h}_1^d, \dots, \mathbf{h}_{N_J}^d]$ and $\mathbf{H}_c = [\mathbf{h}_{1,1}^c, \dots, \mathbf{h}_{N_c, N_J}^c]$, respectively. Additionally, we define the joint probability related to each context map as $\mathbf{p}_{i,n}^c$, where $i = \{1, \dots, N_c\}$ and $n = \{1, \dots, N_J\}$.

Finally, the n^{th} joint position from detection and contextual information aggregated is given by:

$$\mathbf{y}_n = \alpha \mathbf{y}_n^d + (1 - \alpha) \frac{\sum_{i=1}^{N_c} \mathbf{p}_{i,n}^c \mathbf{y}_{i,n}^c}{\sum_{i=1}^{N_c} \mathbf{p}_{i,n}^c}, \quad (6)$$

where $\mathbf{y}_n^d = \text{Soft-argmax}(\mathbf{h}_n^d)$ is the predicted location from the n^{th} part based heat map, $\mathbf{y}_{i,n}^c = \text{Soft-argmax}(\mathbf{h}_{i,n}^c)$ and $\mathbf{p}_{i,n}^c$ are respectively the location and the probability for the i^{th} context heat map for joint n , and α is a hyper-parameter.

From equation (6) we can see that the final prediction is a combination of one specialized prediction and N_c contextual predictions pondered by their probabilities. The contextual weighted contribution brings flexibility, allowing specific filters to be more responsive to particular patterns. This aggregation scheme within the learning stage is only possible because we have the joint probability and position directly available inside the network in a differentiable way.

4. Experiments

We evaluate the proposed method on the very challenging MPII Human Pose [1] and Leeds Sports Poses (LSP) [23] datasets. The MPII dataset contains 25K images collected from YouTube videos, including around 28K annotated poses for training and 15K poses for testing. The annotated poses have 16 body joints, some of them are not present and others are occluded but can be predicted by the context. The LSP dataset is composed by 2000 annotated poses with up to 14 joint locations. The images were gathered from Flickr with sports people. The details about training the model and achieved accuracy results are given as follows.

4.1. Training

The proposed network was trained simultaneously on joints regression and joint probabilities. For joints regression, we use the elastic net loss function (L1 + L2):

$$L_{\mathbf{y}} = \frac{1}{N_J} \sum_{n=1}^{N_J} \|\mathbf{y}_n - \hat{\mathbf{y}}_n\|_1 + \|\mathbf{y}_n - \hat{\mathbf{y}}_n\|_2^2, \quad (7)$$

where \mathbf{y}_n and $\hat{\mathbf{y}}_n$ are respectively the ground truth and the predicted n^{th} joint coordinates. In this case, we use directly the joint coordinates normalized to the interval $[0, 1]$, where the top-left image corner corresponds to $(0, 0)$, and the bottom-right image corner corresponds to $(1, 1)$.

For joint probability estimation, we use the binary cross entropy loss function on the joint probability \mathbf{p} :

$$L_{\mathbf{p}} = \frac{1}{N_J} \sum_{n=1}^{N_J} [(\mathbf{p}_n - 1) \log(1 - \hat{\mathbf{p}}_n) - \mathbf{p}_n \log \hat{\mathbf{p}}_n], \quad (8)$$

where \mathbf{p}_n and $\hat{\mathbf{p}}_n$ are respectively the ground truth and the predicted joint probability.

We optimize the network using back propagation and the RMSProp optimizer, with batch size of 16 samples. For the MPII dataset, we train the network for 120 epochs. The learning rate begins at 10^{-3} and decreases by a factor of 0.4 when accuracy on validation plateaus. We use the same validation split as proposed in [40]. On the LSP dataset, we start from the model trained on MPII and fine-tuned it for more 70 epochs, beginning with learning rate $2 \cdot 10^{-5}$ and using the same decrease procedure. The full training of our network takes three days on the relatively outdated NVIDIA GPU Tesla K20 with 5GB of memory.

Data augmentation. We used standard data augmentation on both MPII and LSP datasets. Input RGB images were cropped and centered on the main subject with a squared bounding box, keeping the people scale (when provided), then resized to 256×256 pixels. We perform random rotations ($\pm 40^\circ$) and random rescaling from 0.7 to 1.3 on MPII and from 0.85 to 1.25 on LSP to make the model more robust to image changes.

Parameters setup. The network model is defined according to Fig. 2 and composed of eight prediction blocks ($K = 8$). We trained the network to regress 16 joints with 2 context maps for each joint ($N_j = 16$, $N_c = 2$). In the aggregation stage, we use $\alpha = 0.8$.

4.2. Results

LSP dataset. We evaluate our method on the LSP dataset using two metrics, the ‘‘Percentage of Correct Parts’’ (PCP) and the ‘‘Probability of Correct Keypoint’’ (PCK) measures, as well as two different evaluation protocols, ‘‘Observer-Centric’’ (OC) and ‘‘Person-Centric’’ (PC), resulting in four different evaluation settings. Our results compared to the state-of-the-art results on the LSP dataset using OC annotations are present in Table 1 (PCK measure) and Table 2 (PCP measure). In both cases, we overcome the best scores by a significant margin, specially with respect to the lower leg and the ankles, on which we increase the results of Pishchulin *et al.* [33] by 6.3% and 4.6%, respectively. To the best of our knowledge, we are the sole regression method to report results using this evaluation settings.

Using the PC annotations on LSP, we achieved the best results among regression based approaches and the second general score, as presented in Tables 3 and 4. On the PCK measure, we outperform the results reported by Carreira *et*

Table 1: Results on LSP test samples using the PCK measure at 0.2 with OC annotations.

| Method | Head | Sho. | Elb. | Wri. | Hip | Knee | Ank. | PCK |
|--------------------------------|-------------|-------------|-------------|-------------|-------------|-------------|-------------|-------------|
| Detection based methods | | | | | | | | |
| Kiefel and Gehler [24] | 83.5 | 73.7 | 55.9 | 36.2 | 73.7 | 70.5 | 66.9 | 65.8 |
| Ramakrishna <i>et al.</i> [35] | 84.9 | 77.8 | 61.4 | 47.2 | 73.6 | 69.1 | 68.8 | 69.0 |
| Pishchulin <i>et al.</i> [32] | 87.5 | 77.6 | 61.4 | 47.6 | 79.0 | 75.2 | 68.4 | 71.0 |
| Ouyang <i>et al.</i> [28] | 86.5 | 78.2 | 61.7 | 49.3 | 76.9 | 70.0 | 67.6 | 70.0 |
| Chen and Yuille [7] | 91.5 | 84.7 | 70.3 | 63.2 | 82.7 | 78.1 | 72.0 | 77.5 |
| Yang <i>et al.</i> [44] | 90.6 | 89.1 | 80.3 | 73.5 | 85.5 | 82.8 | 68.8 | 81.5 |
| Chu <i>et al.</i> [12] | 93.7 | 87.2 | 78.2 | 73.8 | 88.2 | 83.0 | 80.9 | 83.6 |
| Pishchulin <i>et al.</i> [33] | 97.4 | 92.0 | 83.8 | 79.0 | 93.1 | 88.3 | 83.7 | 88.2 |
| Regression based method | | | | | | | | |
| Our method | 97.4 | 93.8 | 86.8 | 82.3 | 93.7 | 90.9 | 88.3 | 90.5 |

Table 2: Results on LSP test samples using the PCP measure with OC annotations.

| Method | Torso | Upper leg | Lower leg | Upper arm | Fore-arm | Head | PCP |
|--------------------------------|-------------|-------------|-------------|-------------|-------------|-------------|-------------|
| Detection based methods | | | | | | | |
| Kiefel and Gehler [24] | 84.3 | 74.5 | 67.6 | 54.1 | 28.3 | 78.3 | 61.2 |
| Pishchulin <i>et al.</i> [31] | 87.4 | 75.7 | 68.0 | 54.4 | 33.7 | 77.4 | 62.8 |
| Ramakrishna <i>et al.</i> [35] | 88.1 | 79.0 | 73.6 | 62.8 | 39.5 | 80.4 | 67.8 |
| Ouyang <i>et al.</i> [28] | 88.6 | 77.8 | 71.9 | 61.9 | 45.4 | 84.3 | 68.7 |
| Pishchulin <i>et al.</i> [32] | 88.7 | 78.9 | 73.2 | 61.8 | 45.0 | 85.1 | 69.2 |
| Chen and Yuille [7] | 92.7 | 82.9 | 77.0 | 69.2 | 55.4 | 87.8 | 75.0 |
| Yang <i>et al.</i> [44] | 96.5 | 88.7 | 81.7 | 78.8 | 66.7 | 83.1 | 81.1 |
| Chu <i>et al.</i> [12] | 95.4 | 87.6 | 83.2 | 76.9 | 65.2 | 89.6 | 81.1 |
| Pishchulin <i>et al.</i> [33] | 96.0 | 91.0 | 83.5 | 82.8 | 71.8 | 96.2 | 85.0 |
| Regression based method | | | | | | | |
| Our method | 98.2 | 93.8 | 89.8 | 85.8 | 75.5 | 96.0 | 88.4 |

Table 3: Results on LSP test samples using the PCK measure at 0.2 with PC annotations.

| Method | Head | Sho. | Elb. | Wri. | Hip | Knee | Ank. | PCK |
|---------------------------------|-------------|-------------|-------------|-------------|-------------|-------------|-------------|-------------|
| Detection based methods | | | | | | | | |
| Pishchulin <i>et al.</i> [32] | 87.2 | 56.7 | 46.7 | 38.0 | 61.0 | 57.5 | 52.7 | 57.1 |
| Chen and Yuille [7] | 91.8 | 78.2 | 71.8 | 65.5 | 73.3 | 70.2 | 63.4 | 73.4 |
| Fan <i>et al.</i> [15] | 92.4 | 75.2 | 65.3 | 64.0 | 75.7 | 68.3 | 70.4 | 73.0 |
| Tompson <i>et al.</i> [41] | 90.6 | 79.2 | 67.9 | 63.4 | 69.5 | 71.0 | 64.2 | 72.3 |
| Yang <i>et al.</i> [44] | 90.6 | 78.1 | 73.8 | 68.8 | 74.8 | 69.9 | 58.9 | 73.6 |
| Rafi <i>et al.</i> [34] | 95.8 | 86.2 | 79.3 | 75.0 | 86.6 | 83.8 | 79.8 | 83.8 |
| Yu <i>et al.</i> [46] | 87.2 | 88.2 | 82.4 | 76.3 | 91.4 | 85.8 | 78.7 | 84.3 |
| Belag. and Ziss. [4] | 95.2 | 89.0 | 81.5 | 77.0 | 83.7 | 87.0 | 82.8 | 85.2 |
| Lifshitz <i>et al.</i> [26] | 96.8 | 89.0 | 82.7 | 79.1 | 90.9 | 86.0 | 82.5 | 86.7 |
| Pishchulin <i>et al.</i> [33] | 97.0 | 91.0 | 83.8 | 78.1 | 91.0 | 86.7 | 82.0 | 87.1 |
| Insafutdinov <i>et al.</i> [21] | 97.4 | 92.7 | 87.5 | 84.4 | 91.5 | 89.9 | 87.2 | 90.1 |
| Wei <i>et al.</i> [43] | 97.8 | 92.5 | 87.0 | 83.9 | 91.5 | 90.8 | 89.9 | 90.5 |
| Bulat and Tzimi. [5] | 97.2 | 92.1 | 88.1 | 85.2 | 92.2 | 91.4 | 88.7 | 90.7 |
| Chu <i>et al.</i> [13] | 98.1 | 93.7 | 89.3 | 86.9 | 93.4 | 94.0 | 92.5 | 92.6 |
| Regression based methods | | | | | | | | |
| Carreira <i>et al.</i> [6] | 90.5 | 81.8 | 65.8 | 59.8 | 81.6 | 70.6 | 62.0 | 73.1 |
| Our method | 97.5 | 93.3 | 87.6 | 84.6 | 92.8 | 92.0 | 90.0 | 91.1 |

al. [6] (CVPR 2016), which is the only regression method reported on this setup, by 18.0%.

MPII dataset. On the MPII dataset, we evaluate our method using the ‘‘Single person’’ challenge [1]. The scores were computed by the providers of the dataset, since the test labels are not publicly available. As shown in Table 5, we reached a test score of 91.2%, which is only 0.7% lower than the best result using detection based method, and 4.8%

Table 4: Results on LSP test samples using the PCP measure with PC annotations.

| Method | Torso | Upper leg | Lower leg | Upper arm | Fore-arm | Head | PCP |
|---------------------------------|-------------|-------------|-------------|-------------|-------------|-------------|-------------|
| Detection based methods | | | | | | | |
| Pishchulin <i>et al.</i> [32] | 88.7 | 63.6 | 58.4 | 46.0 | 35.2 | 85.1 | 58.0 |
| Tompson <i>et al.</i> [41] | 90.3 | 70.4 | 61.1 | 63.0 | 51.2 | 83.7 | 66.6 |
| Fan <i>et al.</i> [15] | 95.4 | 77.7 | 69.8 | 62.8 | 49.1 | 86.6 | 70.1 |
| Chen and Yuille [7] | 96.0 | 77.2 | 72.2 | 69.7 | 58.1 | 85.6 | 73.6 |
| Yang <i>et al.</i> [44] | 95.6 | 78.5 | 71.8 | 72.2 | 61.8 | 83.9 | 74.8 |
| Rafi <i>et al.</i> [34] | 97.6 | 87.3 | 80.2 | 76.8 | 66.2 | 93.3 | 81.2 |
| Belag. and Ziss. [4] | 96.0 | 86.7 | 82.2 | 79.4 | 69.4 | 89.4 | 82.1 |
| Yu <i>et al.</i> [46] | 98.0 | 93.1 | 88.1 | 82.9 | 72.6 | 83.0 | 85.4 |
| Lifshitz <i>et al.</i> [26] | 97.3 | 88.8 | 84.4 | 80.6 | 71.4 | 94.8 | 84.3 |
| Pishchulin <i>et al.</i> [33] | 97.0 | 88.8 | 82.0 | 82.4 | 71.8 | 95.8 | 84.3 |
| Insafutdinov <i>et al.</i> [21] | 97.0 | 90.6 | 86.9 | 86.1 | 79.5 | 95.4 | 87.8 |
| Wei <i>et al.</i> [43] | 98.0 | 92.2 | 89.1 | 85.8 | 77.9 | 95.0 | 88.3 |
| Bulat and Tzimi. [5] | 97.7 | 92.4 | 89.3 | 86.7 | 79.7 | 95.2 | 88.9 |
| Chu <i>et al.</i> [13] | 98.4 | 95.0 | 92.8 | 88.5 | 81.2 | 95.7 | 90.9 |
| Regression based methods | | | | | | | |
| Carreira <i>et al.</i> [6] | 95.3 | 81.8 | 73.3 | 66.7 | 51.0 | 84.4 | 72.5 |
| Our method | 98.2 | 93.6 | 91.0 | 86.6 | 78.2 | 96.8 | 89.4 |

higher than the second score using regression.

Taking into account the competitiveness of the MPII Human Pose challenge², our score represents a very significant improvement over regression based approaches and a promising result compared to detection based methods. Moreover, our method is much simpler than the stacked hourglass network from Newell *et al.* [27] or its extension from Chu *et al.* [13]. Due to limited memory resources, we were not able to train these two models in our hardware. Despite that, we reach comparable results with a model that fits in much smaller GPUs.

4.3. Discussion

As suggested in Section 3.2.1, the proposed *Soft-argmax* function acts as a constrain on the regression approach, driving the network to learn part-based detectors indirectly. This effect provides the flexibility of regression based methods, which can be easily integrated to provide 2D pose estimation to other applications such as 3D pose estimation or action recognition, while preserving the performance of detection based methods. Some examples of part-based maps indirectly learned by our method are show in Fig. 5. As we can see, the responses are very well localized on the true location of the joints without explicitly requiring so.

Additionally to the part-based maps, the contextual maps give extra information to refine the predicted pose. In some cases, the contextual maps provide strong responses to regions around the joint location. In such cases, the aggregation scheme is able to refine the predicted joint position. On the other hand, if the contextual map response is weak, the context reflects in very few changes on the pose. Some examples of predicted poses and visual contributions from

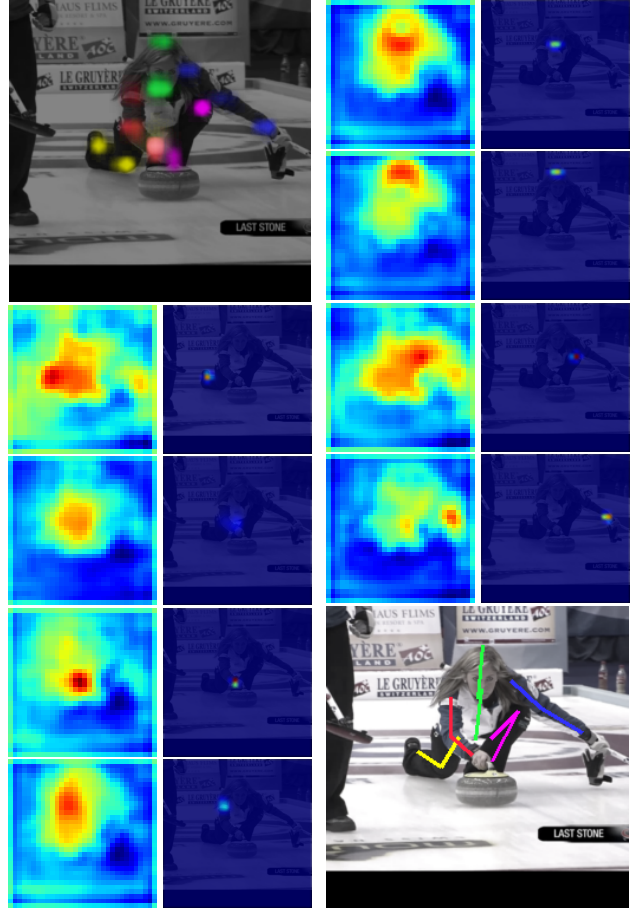


Figure 5: Indirectly learned part-based heat maps from our method. All the joints encoded to RGB are shown in the first image (top-left corner) and the final pose is shown in the last image (bottom-right corner). On each column, the intermediate images correspond to the predicted heat maps before (left) and after (right) the Softmax normalization. The presented heat maps correspond to *right ankle, right hip, right wrist, right shoulder, upper neck, head top, left knee, and left wrist*.

contextual aggregation are shown in Fig. 6. The contextual maps are able to increase the precision of the predictions by providing complementary information, as we can see for the right elbows of the poses in Fig. 6.

5. Conclusion

In this work, we presented a new regression method for human pose estimation from still images. The method is based on the *Soft-argmax* operation, a differentiable operation that can be integrated in a deep convolutional network to learn part-based detection maps indirectly, resulting in a significant improvement over the state-of-the-art scores from regression methods and very competitive re-

²MPII Leader Board: <http://human-pose.mpi-inf.mpg.de>

Table 5: Comparison results with state-of-the-art methods on the MPII dataset on testing, using PCKh measure with threshold as 0.5 of the head segment length. Detection based methods are shown on top and regression based methods on bottom.

| Method | Head | Shoulder | Elbow | Wrist | Hip | Knee | Ankle | Total |
|---------------------------------|-------------|-------------|-------------|-------------|-------------|-------------|-------------|-------------|
| Detection based methods | | | | | | | | |
| Pishchulin <i>et al.</i> [32] | 74.3 | 49.0 | 40.8 | 34.1 | 36.5 | 34.4 | 35.2 | 44.1 |
| Tompson <i>et al.</i> [41] | 95.8 | 90.3 | 80.5 | 74.3 | 77.6 | 69.7 | 62.8 | 79.6 |
| Tompson <i>et al.</i> [40] | 96.1 | 91.9 | 83.9 | 77.8 | 80.9 | 72.3 | 64.8 | 82.0 |
| Hu and Ramanan [20] | 95.0 | 91.6 | 83.0 | 76.6 | 81.9 | 74.5 | 69.5 | 82.4 |
| Pishchulin <i>et al.</i> [33] | 94.1 | 90.2 | 83.4 | 77.3 | 82.6 | 75.7 | 68.6 | 82.4 |
| Lifshitz <i>et al.</i> [26] | 97.8 | 93.3 | 85.7 | 80.4 | 85.3 | 76.6 | 70.2 | 85.0 |
| Gkioxary <i>et al.</i> [17] | 96.2 | 93.1 | 86.7 | 82.1 | 85.2 | 81.4 | 74.1 | 86.1 |
| Rafi <i>et al.</i> [34] | 97.2 | 93.9 | 86.4 | 81.3 | 86.8 | 80.6 | 73.4 | 86.3 |
| Belagiannis and Zisserman [4] | 97.7 | 95.0 | 88.2 | 83.0 | 87.9 | 82.6 | 78.4 | 88.1 |
| Insafutdinov <i>et al.</i> [21] | 96.8 | 95.2 | 89.3 | 84.4 | 88.4 | 83.4 | 78.0 | 88.5 |
| Wei <i>et al.</i> [43] | 97.8 | 95.0 | 88.7 | 84.0 | 88.4 | 82.8 | 79.4 | 88.5 |
| Bulat and Tzimiropoulos [5] | 97.9 | 95.1 | 89.9 | 85.3 | 89.4 | 85.7 | 81.7 | 89.7 |
| Newell <i>et al.</i> [27] | 98.2 | 96.3 | 91.2 | 87.1 | 90.1 | 87.4 | 83.6 | 90.9 |
| Chu <i>et al.</i> [13] | 98.5 | 96.3 | 91.9 | 88.1 | 90.6 | 88.0 | 85.0 | 91.5 |
| Chou <i>et al.</i> [11] | 98.2 | 96.8 | 92.2 | 88.0 | 91.3 | 89.1 | 84.9 | 91.8 |
| Chen <i>et al.</i> [8] | 98.1 | 96.5 | 92.5 | 88.5 | 90.2 | 89.6 | 86.0 | 91.9 |
| Regression based methods | | | | | | | | |
| Rogez <i>et al.</i> [36] | – | – | – | – | – | – | – | 74.2 |
| Carreira <i>et al.</i> [6] | 95.7 | 91.7 | 81.7 | 72.4 | 82.8 | 73.2 | 66.4 | 81.3 |
| Sun <i>et al.</i> [38] | 97.5 | 94.3 | 87.0 | 81.2 | 86.5 | 78.5 | 75.4 | 86.4 |
| Our method | 98.1 | 96.6 | 92.0 | 87.5 | 90.6 | 88.0 | 82.7 | 91.2 |

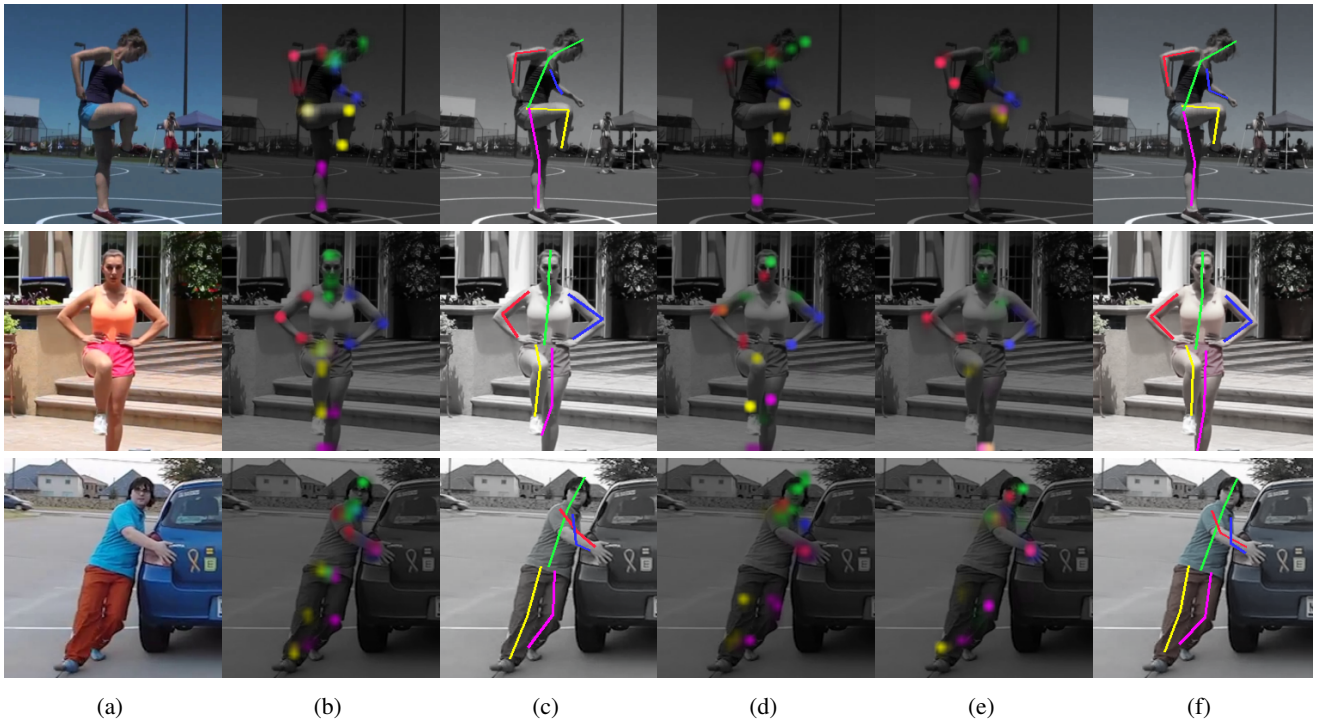


Figure 6: Samples of context maps aggregated to refine predicted pose. Input image (a), part-based detection maps (b), predicted pose without context (c), two different context maps (d) and (e), and the final pose with aggregated predictions (f).

sults compared to detection based approaches. Additionally, we demonstrate that contextual information can be seamlessly integrated into our framework by using additional context maps and joint probabilities. As a future work, other methods could be built up to our approach to provide 3D pose estimation or human action recognition from pose in a fully differentiable way.

Acknowledgment

This work was partially supported by the Brazilian National Council for Scientific and Technological Development (CNPq) – Grant 233342/2014-1.

References

- [1] M. Andriluka, L. Pishchulin, P. Gehler, and B. Schiele. 2D Human Pose Estimation: New Benchmark and State of the Art Analysis. In *IEEE Conference on Computer Vision and Pattern Recognition (CVPR)*, June 2014.
- [2] M. Andriluka, S. Roth, and B. Schiele. Pictorial structures revisited: People detection and articulated pose estimation. In *Computer Vision and Pattern Recognition (CVPR)*, pages 1014–1021, June 2009.
- [3] V. Belagiannis, C. Rupprecht, G. Carneiro, and N. Navab. Robust optimization for deep regression. In *International Conference on Computer Vision (ICCV)*, pages 2830–2838, Dec 2015.
- [4] V. Belagiannis and A. Zisserman. Recurrent human pose estimation. *CoRR*, abs/1605.02914, 2016.
- [5] A. Bulat and G. Tzimiropoulos. Human pose estimation via Convolutional Part Heatmap Regression. In *European Conference on Computer Vision (ECCV)*, pages 717–732, 2016.
- [6] J. Carreira, P. Agrawal, K. Fragkiadaki, and J. Malik. Human pose estimation with iterative error feedback. In *2016 IEEE Conference on Computer Vision and Pattern Recognition (CVPR)*, pages 4733–4742, June 2016.
- [7] X. Chen and A. Yuille. Articulated pose estimation by a graphical model with image dependent pairwise relations. In *Advances in Neural Information Processing Systems (NIPS)*, 2014.
- [8] Y. Chen, C. Shen, X. Wei, L. Liu, and J. Yang. Adversarial posenet: A structure-aware convolutional network for human pose estimation. *CoRR*, abs/1705.00389, 2017.
- [9] F. Chollet. Xception: Deep learning with depthwise separable convolutions. *CoRR*, abs/1610.02357, 2016.
- [10] F. Chollet et al. Keras. <https://github.com/fchollet/keras>, 2015.
- [11] C. Chou, J. Chien, and H. Chen. Self adversarial training for human pose estimation. *CoRR*, abs/1707.02439, 2017.
- [12] X. Chu, W. Ouyang, H. Li, and X. Wang. Structured feature learning for pose estimation. In *Computer Vision and Pattern Recognition (CVPR)*, 2016.
- [13] X. Chu, W. Yang, W. Ouyang, C. Ma, A. L. Yuille, and X. Wang. Multi-context attention for human pose estimation. *arXiv preprint arXiv:1702.07432*, 2017.
- [14] M. Dantone, J. Gall, C. Leistner, and L. V. Gool. Human Pose Estimation Using Body Parts Dependent Joint Regressors. In *Computer Vision and Pattern Recognition (CVPR)*, pages 3041–3048, June 2013.
- [15] X. Fan, K. Zheng, Y. Lin, and S. Wang. Combining local appearance and holistic view: Dual-source deep neural networks for human pose estimation. In *The IEEE Conference on Computer Vision and Pattern Recognition (CVPR)*, June 2015.
- [16] P. F. Felzenszwalb and D. P. Huttenlocher. Pictorial structures for object recognition. *International Journal of Computer Vision*, 61(1):55–79, 2005.
- [17] G. Gkioxari, A. Toshev, and N. Jaitly. Chained Predictions Using Convolutional Neural Networks. *European Conference on Computer Vision (ECCV)*, 2016.
- [18] K. He, X. Zhang, S. Ren, and J. Sun. Deep residual learning for image recognition. In *The IEEE Conference on Computer Vision and Pattern Recognition (CVPR)*, June 2016.
- [19] K. He, X. Zhang, S. Ren, and J. Sun. Deep Residual Learning for Image Recognition. In *IEEE Conference on Computer Vision and Pattern Recognition (CVPR)*, 2016.
- [20] P. Hu and D. Ramanan. Bottom-up and top-down reasoning with convolutional latent-variable models. In *2016 IEEE Conference on Computer Vision and Pattern Recognition (CVPR)*. 2016.
- [21] E. Insafutdinov, L. Pishchulin, B. Andres, M. Andriluka, and B. Schiele. DeeperCut: A Deeper, Stronger, and Faster Multi-Person Pose Estimation Model. In *European Conference on Computer Vision (ECCV)*, May 2016.
- [22] C. Ionescu, F. Li, and C. Sminchisescu. Latent structured models for human pose estimation. In *International Conference on Computer Vision (ICCV)*, pages 2220–2227, Nov 2011.
- [23] S. Johnson and M. Everingham. Clustered pose and nonlinear appearance models for human pose estimation. In *Proceedings of the British Machine Vision Conference*, 2010.
- [24] M. Kiefel and P. V. Gehler. *Human Pose Estimation with Fields of Parts*, pages 331–346. Springer International Publishing, Cham, 2014.
- [25] L. Ladicky, P. H. S. Torr, and A. Zisserman. Human pose estimation using a joint pixel-wise and part-wise formulation. In *Computer Vision and Pattern Recognition (CVPR)*, 2013.
- [26] I. Lifshitz, E. Fetaya, and S. Ullman. *Human Pose Estimation Using Deep Consensus Voting*, pages 246–260. Springer International Publishing, Cham, 2016.
- [27] A. Newell, K. Yang, and J. Deng. Stacked Hourglass Networks for Human Pose Estimation. *European Conference on Computer Vision (ECCV)*, pages 483–499, 2016.
- [28] W. Ouyang, X. Chu, and X. Wang. Multi-source deep learning for human pose estimation. In *Computer Vision and Pattern Recognition (CVPR)*, pages 2337–2344, June 2014.
- [29] T. Pfister, J. Charles, and A. Zisserman. Flowing convnets for human pose estimation in videos. In *International Conference on Computer Vision (ICCV)*, 2015.
- [30] T. Pfister, K. Simonyan, J. Charles, and A. Zisserman. Deep convolutional neural networks for efficient pose estimation in gesture videos. In *Asian Conference on Computer Vision (ACCV)*, 2014.

- [31] L. Pishchulin, M. Andriluka, P. Gehler, and B. Schiele. Poselet Conditioned Pictorial Structures. In *Computer Vision and Pattern Recognition (CVPR)*, pages 588–595, June 2013.
- [32] L. Pishchulin, M. Andriluka, P. V. Gehler, and B. Schiele. Strong appearance and expressive spatial models for human pose estimation. In *International Conference on Computer Vision (ICCV)*, pages 3487–3494, 2013.
- [33] L. Pishchulin, E. Insafutdinov, S. Tang, B. Andres, M. Andriluka, P. Gehler, and B. Schiele. DeepCut: Joint Subset Partition and Labeling for Multi Person Pose Estimation. In *IEEE Conference on Computer Vision and Pattern Recognition (CVPR)*, June 2016.
- [34] U. Rafi, I. Kostrikov, J. Gall, and B. Leibe. An efficient convolutional network for human pose estimation. In *BMVC*, volume 1, page 2, 2016.
- [35] V. Ramakrishna, D. Munoz, M. Hebert, A. J. Bagnell, and Y. Sheikh. Pose Machines: Articulated Pose Estimation via Inference Machines. In *European Conference on Computer Vision (ECCV)*, 2014.
- [36] G. Rogez, P. Weinzaepfel, and C. Schmid. LCR-Net: Localization-Classification-Regression for Human Pose. In *Conference on Computer Vision and Pattern Recognition (CVPR)*, June 2017.
- [37] K. Simonyan and A. Zisserman. Very deep convolutional networks for large-scale image recognition. In *International Conference on Learning Representations*, 2015.
- [38] X. Sun, J. Shang, S. Liang, and Y. Wei. Compositional human pose regression. *arXiv preprint arXiv:1702.07432*, 2017.
- [39] C. Szegedy, S. Ioffe, and V. Vanhoucke. Inception-v4, inception-resnet and the impact of residual connections on learning. *CoRR*, abs/1602.07261, 2016.
- [40] J. Tompson, R. Goroshin, A. Jain, Y. LeCun, and C. Bregler. Efficient object localization using Convolutional Networks. In *IEEE Conference on Computer Vision and Pattern Recognition (CVPR)*, pages 648–656, June 2015.
- [41] J. J. Tompson, A. Jain, Y. LeCun, and C. Bregler. Joint training of a convolutional network and a graphical model for human pose estimation. In Z. Ghahramani, M. Welling, C. Cortes, N. D. Lawrence, and K. Q. Weinberger, editors, *Advances in Neural Information Processing Systems 27*, pages 1799–1807. Curran Associates, Inc., 2014.
- [42] A. Toshev and C. Szegedy. DeepPose: Human Pose Estimation via Deep Neural Networks. In *Computer Vision and Pattern Recognition (CVPR)*, pages 1653–1660, 2014.
- [43] S.-E. Wei, V. Ramakrishna, T. Kanade, and Y. Sheikh. Convolutional pose machines. In *IEEE Conference on Computer Vision and Pattern Recognition (CVPR)*, 2016.
- [44] W. Yang, W. Ouyang, H. Li, and X. Wang. End-to-end learning of deformable mixture of parts and deep convolutional neural networks for human pose estimation. In *Computer Vision and Pattern Recognition (CVPR)*, 2016.
- [45] Y. Yang, S. Baker, A. Kannan, and D. Ramanan. Recognizing proxemics in personal photos. In *2012 IEEE Conference on Computer Vision and Pattern Recognition*, pages 3522–3529, June 2012.
- [46] X. Yu, F. Zhou, and M. Chandraker. *Deep Deformation Network for Object Landmark Localization*, pages 52–70. Springer International Publishing, Cham, 2016.